

Dynamic spin susceptibility in the t - J model

A. A. Vladimirov^a, D. Ihle^b, and N. M. Plakida^{a,c}

^aJoint Institute for Nuclear Research, 141980 Dubna, Russia

^bInstitut für Theoretische Physik, Universität Leipzig, D-04109, Leipzig, Germany

^cMax-Planck-Institut für Physik komplexer Systeme, D-01187, Dresden, Germany

(Dated: November 9, 2018)

A relaxation-function theory for the dynamic spin susceptibility in the t - J model is presented. By a sum-rule-conserving generalized mean-field approximation (GMFA), the two-spin correlation functions of arbitrary range, the staggered magnetization, the uniform static susceptibility, and the antiferromagnetic correlation length are calculated in a wide region of hole doping and temperatures. A good agreement with available exact diagonalization (ED) data is found. The correlation length is in reasonable agreement with neutron-scattering experiments on $\text{La}_{2-\delta}\text{Sr}_\delta\text{CuO}_4$. Going beyond the GMFA, the self-energy is calculated in the mode-coupling approximation. The spin dynamics at arbitrary frequencies and wave vectors is studied for various temperatures and hole doping. At low doping a spin-wave-type behavior is found as in the Heisenberg model, while at higher doping a strong damping caused by hole hopping occurs, and a relaxation-type spin dynamics is observed in agreement with the ED results. The local spin susceptibility and its ω/T scaling behavior are calculated in a reasonable agreement with experimental and ED data.

PACS numbers: 74.72.-h, 75.10.-b, 75.40.Gb

I. INTRODUCTION

It is generally believed that charge-carrier interaction with spin fluctuations in the cuprate high-temperature superconductors is the origin of their anomalous normal state properties and may be responsible for the superconducting transition (see, e.g., Ref. [1]). Inelastic neutron scattering experiments have revealed quite a complicated behavior of the spin-fluctuation spectra in cuprates. [2, 3] Therefore, studies of spin fluctuations in these materials are essential in elucidating the nature of high-temperature superconductivity. Two limiting cases can be well described. In the undoped insulating phase the quasi-two-dimensional Heisenberg model for localized spins gives a reasonable description of the spin-fluctuation spectra (see, e.g., Ref. [4]), while in the overdoped region the random phase approximation (RPA) for weakly correlated itinerant electrons can be applied (see, e.g., Ref. [5]).

However, the region of light and optimal doping (the so-called “pseudogap phase”), where localized spins on copper sites strongly interact with correlated charge carriers is much more difficult to study. This region should be treated within a model of strongly correlated electrons like the Hubbard model [6] or the t - J model.[7] The charge-carrier motion in the t - J model is described by the Hubbard projection operators, whose commutation relations are more complicated than those of Fermi or Bose operators. Various approaches have been used to study the spin dynamics in the t - J model (for a review see, e.g., Refs. [8] and [9]). In particular, in the slave boson or fermion methods, a local constraint prohibiting a double occupancy of any quantum state is difficult to treat rigorously. An application of a special diagram technique for Hubbard operators to the t - J model results in a complicated analytical expression for the dynamic spin suscep-

tibility (DSS). [10] Studies of finite clusters by numerical methods were important in elucidating static and dynamic spin interactions, though they have limited energy and momentum resolutions (see, e.g., Refs. [11, 12, 13]).

To overcome this complexity, we apply the projection Mori-type technique elaborated for the two-time thermodynamic Green’s function (GF). [14, 15, 16] In this method an exact representation for the self-energy (or polarization operator) can be derived which, when evaluated in the mode-coupling approximation, yields physically reasonable results even for strongly interacting systems. As our calculations have shown, the decoupling of the correlation function of currents, i.e., $(dS_{\mathbf{q}}^+/dt)$, in Ref. [17] is insufficient for obtaining reasonable results. Therefore, in the present paper, in studying the DSS $\chi(\mathbf{q}, \omega) = -\langle\langle S_{\mathbf{q}}^+ | S_{-\mathbf{q}}^- \rangle\rangle_\omega$ (written in terms of the GF [14]) the mode-coupling approximation in the paramagnetic phase is applied to the correlation functions of the forces, i.e., $(d^2 S_{\mathbf{q}}^+/dt^2)$. [16] A similar approach based on the Mori projection technique for the single-particle electron GF and spin GF has been used in Refs. [18, 19, 20, 21]. The magnetic resonance mode observed in the superconducting state was studied within the memory-function approach in Refs. [20, 22, 23, 24].

In this paper we use the spin-rotation-invariant relaxation-function theory for the DSS in the t - J model derived by us in Ref. [25] to calculate the static properties in the generalized mean-field approximation (GMFA) similarly to Ref. [26] and the dynamic spin-fluctuation spectra using the mode-coupling approximation for the force-force correlation functions. Thereby, we capture both the local and itinerant character of charge carriers in a consistent way. In calculating the static properties, in particular the static susceptibility and spin-excitation spectrum, we pay particular attention to a proper description of antiferromagnetic (AF) short-range

order (SRO) and its implications on the spin dynamics. For the undoped case described by the Heisenberg model our results are similar to those in Refs. [27] and [28]. For a finite doping our theory yields a reasonable agreement with available exact diagonalization (ED) data and neutron scattering experiments.

The paper is organized as follows. In the next section the t - J model is formulated in terms of the Hubbard operators, and basic formulas for the static spin susceptibility and the self-energy within the relaxation-function theory [25] are presented. Numerical results for the static properties and spin-fluctuation spectra are given in Sec. III, where their temperature and doping dependences are analyzed. The conclusion is given in Sec. IV. Details of the calculations are discussed in the Appendix.

II. RELAXATION-FUNCTION THEORY

A. Basic formulas

We start with the t - J model on the square lattice,

$$H = - \sum_{i \neq j, \sigma} t_{ij} X_i^{\sigma 0} X_j^{0 \sigma} - \mu \sum_{i \sigma} X_i^{\sigma \sigma} + \frac{1}{4} \sum_{i \neq j, \sigma} J_{ij} (X_i^{\sigma \bar{\sigma}} X_j^{\bar{\sigma} \sigma} - X_i^{\sigma \sigma} X_j^{\bar{\sigma} \bar{\sigma}}), \quad (1)$$

which is written in terms of the Hubbard operators (HOs) [6] $X_i^{\alpha\beta} = |i, \alpha\rangle\langle i, \beta|$ for three possible states at a lattice site i : for an empty site $|i, \alpha\rangle = |i, 0\rangle$ and for a singly occupied site $|i, \alpha\rangle = |i, \sigma\rangle$ with spin $\sigma(1/2)$ ($\sigma = \pm$, $\bar{\sigma} = -\sigma$). The HOs obey the multiplication rule $X_i^{\alpha\beta} X_i^{\beta\gamma} = X_i^{\alpha\gamma}$ and the completeness relation $X_i^{00} + \sum_{\sigma} X_i^{\sigma\sigma} = 1$, which preserves rigorously the constraint of no double-occupancy of any lattice site. The spin and number operators of the model are given by $S_i^{\sigma} = X_i^{\sigma\bar{\sigma}}$, $S_i^z = (1/2) \sum_{\sigma} \sigma X_i^{\sigma\sigma}$, and $n_i = \sum_{\sigma} X_i^{\sigma\sigma}$. The chemical potential μ is determined from the equation for the average electron density $n = \sum_{\sigma} \langle X_i^{\sigma\sigma} \rangle = 1 - \delta$ where $\delta = \langle X_i^{00} \rangle$ is the hole concentration.

In Ref. [25] we have derived the general expression for the DSS $\chi(\mathbf{q}, \omega) = -\langle\langle S_{\mathbf{q}}^+ | S_{-\mathbf{q}}^- \rangle\rangle_{\omega}$,

$$\chi(\mathbf{q}, \omega) = \chi_{\mathbf{q}} \frac{\omega_{\mathbf{q}}^2}{\omega_{\mathbf{q}}^2 + \omega \Sigma(\mathbf{q}, \omega) - \omega^2}. \quad (2)$$

The static spin susceptibility $\chi_{\mathbf{q}}$ is related to a generalized mean-field spin-excitation spectrum $\omega_{\mathbf{q}}$ by the equation

$$\chi_{\mathbf{q}} = (S_{\mathbf{q}}^+, S_{-\mathbf{q}}^-) = m(\mathbf{q})/\omega_{\mathbf{q}}^2 \quad (3)$$

with $m(\mathbf{q}) = \langle\langle [i\dot{S}_{\mathbf{q}}^+, S_{-\mathbf{q}}^-] \rangle\rangle$. Here, the Kubo-Mori scalar product is defined as (see, e.g., Ref. [16])

$$(A(t), B) = \int_0^{\beta} d\lambda \langle A(t - i\lambda) B \rangle, \quad \beta = 1/k_{\text{B}}T. \quad (4)$$

The self-energy is given by [25]

$$\Sigma(\mathbf{q}, \omega) = \frac{1}{m(\mathbf{q})} ((-\ddot{S}_{\mathbf{q}}^+ | -\ddot{S}_{-\mathbf{q}}^-))_{\omega}^{\text{(proper)}}, \quad (5)$$

where

$$((A|B))_{\omega} = -i \int_0^{\infty} dt e^{i\omega t} (A(t), B) \quad (6)$$

is the Kubo-Mori relaxation function and its ‘‘proper’’ part means that it does not contain parts connected by a single relaxation function in the GMFA. The spin-fluctuation spectrum is given by the imaginary part of the DSS (2),

$$\chi''(\mathbf{q}, \omega) = \frac{-\omega \Sigma''(\mathbf{q}, \omega) m(\mathbf{q})}{[\omega^2 - \omega_{\mathbf{q}}^2 - \omega \Sigma'(\mathbf{q}, \omega)]^2 + [\omega \Sigma''(\mathbf{q}, \omega)]^2}, \quad (7)$$

where $\Sigma(\mathbf{q}, \omega + i0^+) = \Sigma'(\mathbf{q}, \omega) + i\Sigma''(\mathbf{q}, \omega)$, and $\Sigma'(\mathbf{q}, \omega) = -\Sigma'(\mathbf{q}, -\omega)$ and $\Sigma''(\mathbf{q}, \omega) = \Sigma''(\mathbf{q}, -\omega) < 0$ are the real and imaginary parts of the self-energy, respectively.

B. Static properties

To calculate the static susceptibility and the spin-excitation spectrum $\omega_{\mathbf{q}}$ in Eq. (3), we use the equality

$$m(\mathbf{q}) = \langle\langle [i\dot{S}_{\mathbf{q}}^+, S_{-\mathbf{q}}^-] \rangle\rangle = (-\ddot{S}_{\mathbf{q}}^+, S_{-\mathbf{q}}^-), \quad (8)$$

where

$$m(\mathbf{q}) = -8t(1 - \gamma_{\mathbf{q}})F_{1,0} - 8J(1 - \gamma_{\mathbf{q}})C_{1,0} \quad (9)$$

with $\gamma_{\mathbf{q}} = (1/2)(\cos q_x + \cos q_y)$ (we take the lattice spacing a to be unity), $F_{n,m} \equiv F_{\mathbf{R}} = \langle X_{\mathbf{0}}^{\sigma 0} X_{\mathbf{R}}^{0\sigma} \rangle$, $C_{n,m} \equiv C_{\mathbf{R}} = \langle S_{\mathbf{0}}^+ S_{\mathbf{R}}^- \rangle$, and $\mathbf{R} = ne_x + me_y$. Here, we take into account the hopping integral t_{ij} and the exchange interaction J_{ij} for the nearest neighbors only denoted by t and J , respectively.

To calculate the correlation function $(-\ddot{S}_{\mathbf{q}}^+, S_{-\mathbf{q}}^-)$ in Eq. (8), we take the site representation and use the decoupling procedure which is equivalent to the mode-coupling approximation for the equal-time correlation function (see Appendix A). We obtain $(-\ddot{S}_{\mathbf{q}}^+, S_{-\mathbf{q}}^-) = \omega_{\mathbf{q}}^2 (S_{\mathbf{q}}^+, S_{-\mathbf{q}}^-)$ and, by comparison with Eq. (3), we get the spin-excitation spectrum

$$\begin{aligned} \omega_{\mathbf{q}}^2 &= 8t^2 \lambda_1 (1 - \gamma_{\mathbf{q}}) (1 - n - F_{2,0} - 2F_{1,1}) \\ &+ 4J^2 (1 - \gamma_{\mathbf{q}}) (\lambda_2 \frac{n}{2} - \alpha_1 C_{1,0} (4\gamma_{\mathbf{q}} + 1) \\ &+ \alpha_2 (2C_{1,1} + C_{2,0})). \end{aligned} \quad (10)$$

The decoupling parameters $\alpha_1, \alpha_2, \lambda_1$, and λ_2 are explained in Appendix A. Thus, the static susceptibility can be calculated from Eq. (3).

The AF correlation length ξ may be calculated by expanding the static susceptibility in the neighborhood of

the AF wave vector $\mathbf{Q} = (\pi, \pi)$, $\chi_{\mathbf{Q}+\mathbf{k}} = \chi_{\mathbf{Q}}/(1 + \xi^2 k^2)$. [27, 29] We get

$$\xi^2 = \frac{8J^2\alpha_1|C_{1,0}|}{\omega_{\mathbf{Q}}^2}. \quad (11)$$

The critical behavior of the model (1) is reflected by the divergence of $\chi_{\mathbf{Q}}$ and ξ as $T \rightarrow 0$, i.e., by $\omega_{\mathbf{Q}}(T=0) = 0$. In the phase with AF long-range order (LRO) which, in two dimensions, may occur at $T=0$ only, the correlation function $C_{\mathbf{R}}$ is written as [27, 29]

$$C_{\mathbf{R}} = \frac{1}{N} \sum_{\mathbf{q} \neq \mathbf{Q}} C_{\mathbf{q}} e^{i\mathbf{q}\mathbf{R}} + C e^{i\mathbf{Q}\mathbf{R}}, \quad (12)$$

where $C_{\mathbf{q}} = \langle S_{\mathbf{q}}^+ S_{-\mathbf{q}}^- \rangle$. The condensation part C determines the staggered magnetization which is defined in the spin-rotation-invariant form

$$m^2 = \frac{3}{2N} \sum_{\mathbf{R}} C_{\mathbf{R}} e^{-i\mathbf{Q}\mathbf{R}} = \frac{3}{2} C. \quad (13)$$

The static susceptibility, the correlation functions, the correlation length, and the magnetization are calculated in the GMFA for arbitrary temperatures and doping (see Sec. III.A). Then, the GMFA results are used for the calculation of the self-energy (see Sec. III.B).

C. Self-energy

The self-energy (5) can be written in terms of the corresponding time-dependent correlation function as

$$\Sigma(\mathbf{q}, \omega) = \frac{1}{2\pi m(\mathbf{q})} \int_{-\infty}^{\infty} d\omega' \frac{e^{\beta\omega'} - 1}{\omega'(\omega - \omega')} \int_{-\infty}^{\infty} dt e^{i\omega't} \langle \ddot{S}_{-\mathbf{q}}^- \ddot{S}_{\mathbf{q}}^+(t) \rangle_{\text{proper}}. \quad (14)$$

The self-energy is calculated in the mode-coupling approximation for the multisite correlation functions resulting from the operator $\ddot{S}_{\mathbf{q}}^+(t)$ as outlined in Appendix B. We consider only the imaginary part of the self-energy (14) since the real part is given by the dispersion relation [14].

As it turns out by numerical evaluations (see Sec. III.B), the largest contributions come from two diagonal terms. For the first term Σ''_J we get

$$\begin{aligned} \Sigma''_J(\mathbf{q}, \omega) &= \frac{\pi(2J)^4}{2m(\mathbf{q})\omega N(\omega)} \frac{1}{N^2} \sum_{\mathbf{q}_1, \mathbf{q}_2} \int_{-\infty}^{\infty} d\omega_1 d\omega_2 \\ &\{ \Gamma_{\mathbf{q}_1 \mathbf{q}_2 \mathbf{q}_3}^2 + \Gamma_{\mathbf{q}_1 \mathbf{q}_2 \mathbf{q}_3} \Gamma_{\mathbf{q}_2 \mathbf{q}_1 \mathbf{q}_3} \} N(\omega_1) N(\omega_2) \\ &N(\omega - \omega_1 - \omega_2) B_{\mathbf{q}_1}(\omega_1) B_{\mathbf{q}_2}(\omega_2) B_{\mathbf{q}_3}(\omega - \omega_1 - \omega_2), \end{aligned} \quad (15)$$

where $N(\omega) = (e^{\beta\omega} - 1)^{-1}$ and $\mathbf{q} = \mathbf{q}_1 + \mathbf{q}_2 + \mathbf{q}_3$. The spectral density of the spin-fluctuation spectrum

$B_{\mathbf{q}}(\omega) = (1/\pi) \chi''(\mathbf{q}, \omega)$ is given by Eq. (7). The vertex for the spin-spin scattering reads (cf. Ref. [28])

$$\begin{aligned} \Gamma_{\mathbf{q}_1 \mathbf{q}_2 \mathbf{q}_3} &= 4(\gamma_{\mathbf{q}_3 + \mathbf{q}_1} - \gamma_{\mathbf{q}_2})(\gamma_{\mathbf{q}_3} - \gamma_{\mathbf{q}_1}) \\ &\quad - \gamma_{\mathbf{q}_1} + \gamma_{\mathbf{q}_3} + \gamma_{\mathbf{q}_2 + \mathbf{q}_3} - \gamma_{\mathbf{q}_2 + \mathbf{q}_1}. \end{aligned} \quad (16)$$

The second term Σ''_t is given by

$$\begin{aligned} \Sigma''_t(\mathbf{q}, \omega) &= \frac{\pi(2t)^4}{m(\mathbf{q})\omega N(\omega)} \frac{1}{N^2} \sum_{\mathbf{q}_1, \mathbf{q}_2} \int_{-\infty}^{\infty} d\omega_1 d\omega_2 \\ &\{ \Lambda_{\mathbf{q}_1 \mathbf{q}_2 \mathbf{q}_3}^2 + \Lambda_{\mathbf{q}_3 \mathbf{q}_2 \mathbf{q}_1}^2 \} N(\omega_2) n(\omega + \omega_1 - \omega_2) [1 - n(\omega_1)] \\ &[(1/4)N_{\mathbf{q}_2}(\omega_2) + B_{\mathbf{q}_2}(\omega_2)] A_{\mathbf{q}_1}(\omega_1) A_{\mathbf{q}_3}(\omega + \omega_1 - \omega_2), \end{aligned} \quad (17)$$

where $n(\omega) = (e^{\beta\omega} + 1)^{-1}$. Here, the single-particle spectral function $A_{\mathbf{q}}(\omega) = -(1/\pi) \text{Im} \langle \langle X_{\mathbf{q}}^{0\sigma} | X_{\mathbf{q}}^{\sigma 0} \rangle \rangle_{\omega}$ and the charge-susceptibility spectral function $N_{\mathbf{q}}(\omega) = -(1/\pi) \text{Im} \langle \langle n_{\mathbf{q}} | n_{-\mathbf{q}} \rangle \rangle_{\omega}$ are introduced. The vertex for the spin-hole scattering reads

$$\Lambda_{\mathbf{q}_1 \mathbf{q}_2 \mathbf{q}_3} = 4(\gamma_{\mathbf{q}_3 + \mathbf{q}_2} - \gamma_{\mathbf{q}_1}) \gamma_{\mathbf{q}_3} + \gamma_{\mathbf{q}_2} - \gamma_{\mathbf{q}_1 + \mathbf{q}_3}. \quad (18)$$

The remaining terms in the self-energy are considered in Appendix B. In Sec. III.B we calculate the diagonal terms for various doping and temperatures.

We would like to emphasize that in our calculation of the self-energy in Eq. (17) contributions from the charge and spin excitations are taken into account explicitly by the spectral densities $N_{\mathbf{q}_2}(\omega_2)$ and $B_{\mathbf{q}_2}(\omega_2)$. Contrary to this, in Refs. [20] and [22] these terms have been approximated by some kind of static or mean-field-type expressions. This results in the self-energy of the form similar to that given by a conventional particle-hole loop diagram used in the weak coupling theory like RPA. This form of the self-energy can be readily obtained from our expression (17), if we disregard the charge fluctuation contribution and neglect a small spin excitation energy ω_2 in comparison with the Fermi energy in the Fermi function and in the hole spectral function: $n(\omega + \omega_1 - \omega_2) A_{\mathbf{q}_3}(\omega + \omega_1 - \omega_2) \simeq n(\omega + \omega_1) A_{\mathbf{q}_3}(\omega + \omega_1)$. Then we can integrate over ω_2 in Eq. (17) which gives $\int_{-\infty}^{\infty} d\omega_2 N(\omega_2) B_{\mathbf{q}_2}(\omega_2) = C_{\mathbf{q}_2}$, where $C_{\mathbf{q}} = \langle S_{\mathbf{q}}^+ S_{-\mathbf{q}}^- \rangle$. As a result the self-energy takes the form

$$\begin{aligned} \Sigma''_t(\mathbf{q}, \omega) &= \frac{\pi(2t)^4}{m(\mathbf{q})\omega} \frac{1}{N^2} \sum_{\mathbf{q}_1, \mathbf{q}_2} C_{\mathbf{q}_2} \{ \Lambda_{\mathbf{q}_1 \mathbf{q}_2 \mathbf{q}_3}^2 + \Lambda_{\mathbf{q}_3 \mathbf{q}_2 \mathbf{q}_1}^2 \} \\ &\int_{-\infty}^{\infty} d\omega_1 [n(\omega + \omega_1) - n(\omega_1)] A_{\mathbf{q}_1}(\omega_1) A_{\mathbf{q}_3}(\omega + \omega_1), \end{aligned} \quad (19)$$

which is similar to that found in the one-loop particle-hole approximation used in Refs. [18]-[20] and [22] and describes the damping due to the decay of spin fluctuations into electron-hole excitations. The same result can be deduced, if in the mode-coupling approximation (see Appendix, Eq. (B2)) the time-dependent spin correlation function is approximated by its static value: $\langle X_{\mathbf{k}_2}^{\sigma\sigma}(t) X_{-\mathbf{k}_2}^{\sigma\sigma} \rangle \approx \langle X_{\mathbf{k}_2}^{\sigma\sigma} X_{-\mathbf{k}_2}^{\sigma\sigma} \rangle$. As our numerical calculations have shown, the imaginary part of the self-energy (19) is about twice as large in comparison with that given by Eq. (17).

III. NUMERICAL RESULTS

To investigate the magnetic properties of the t - J model, in particular the spin dynamics at arbitrary temperatures and hole concentrations, we start from the GMFA. By Eq. (2) we get the DSS

$$\chi^{(0)}(\mathbf{q}, \omega) = \frac{m(\mathbf{q})}{2\omega_{\mathbf{q}}} \left(\frac{1}{\omega + \omega_{\mathbf{q}}} - \frac{1}{\omega - \omega_{\mathbf{q}}} \right) \quad (20)$$

with $m(\mathbf{q})$ and $\omega_{\mathbf{q}}$ given by Eqs. (9) and (10), respectively, and the correlation function

$$C_{\mathbf{q}} = \langle S_{\mathbf{q}}^+ S_{-\mathbf{q}}^- \rangle = \frac{m(\mathbf{q})}{2\omega_{\mathbf{q}}} \coth \frac{\beta\omega_{\mathbf{q}}}{2}. \quad (21)$$

The electron Green function is calculated in the Hubbard I approximation which yields

$$\langle\langle X_{\mathbf{q}}^{0\sigma} | X_{\mathbf{q}}^{\sigma 0} \rangle\rangle_{\omega} = \frac{1 - n/2}{\omega - E_{\mathbf{q}} + \mu} \quad (22)$$

with $E_{\mathbf{q}} = -4(1 - n/2)t\gamma_{\mathbf{q}}$. We get

$$F_{\mathbf{q}} = \langle X_{\mathbf{q}}^{\sigma 0} X_{\mathbf{q}}^{0\sigma} \rangle = (1 - n/2)n(E_{\mathbf{q}} - \mu). \quad (23)$$

The chemical potential μ is calculated by the number condition $n = (2/N) \sum_{\mathbf{q}} F_{\mathbf{q}}$.

To go one step beyond the GMFA, we calculate the self-energy [Eqs. (15)-(18)] by inserting the GMFA results. Moreover, for the spectral function $N_{\mathbf{q}}(\omega)$ of the dynamic charge susceptibility appearing in Eq. (17) we take the GMFA result of Ref. [30]:

$$N_{\mathbf{q}}^{(0)}(\omega) = 8tF_{1,0}(1 - \gamma_{\mathbf{q}}) \times (1/\Omega_{\mathbf{q}})[\delta(\omega - \Omega_{\mathbf{q}}) - \delta(\omega + \Omega_{\mathbf{q}})], \quad (24)$$

where $\Omega_{\mathbf{q}}^2 = 8t^2(1 - \gamma_{\mathbf{q}})(1 - n/2)$ in the leading order of doping.

A. Static properties

Considering first the static magnetic properties in the GMFA, we have to solve numerically the coupled system of self-consistency equations for the correlation functions $C_{\mathbf{R}} = (1/N) \sum_{\mathbf{q}} C_{\mathbf{q}} e^{i\mathbf{q}\mathbf{R}}$ and for the transfer amplitudes $F_{\mathbf{R}} = (1/N) \sum_{\mathbf{q}} F_{\mathbf{q}} e^{i\mathbf{q}\mathbf{R}}$. In the long-range ordered phase, Eq. (12) and the additional equation $\omega_{\mathbf{Q}} = 0$ determining the condensation part C must be taken into account. To this end, the parameters α_1 , α_2 , λ_1 , and λ_2 have to be determined, where the sum rule

$$C_{0,0} = \langle S_0^+ S_0^- \rangle = \frac{1}{2}(1 - \delta) \quad (25)$$

must be fulfilled at arbitrary temperatures and hole doping.

We fix the decoupling parameters as follows. The parameters α_1 and α_2 are determined in the Heisenberg

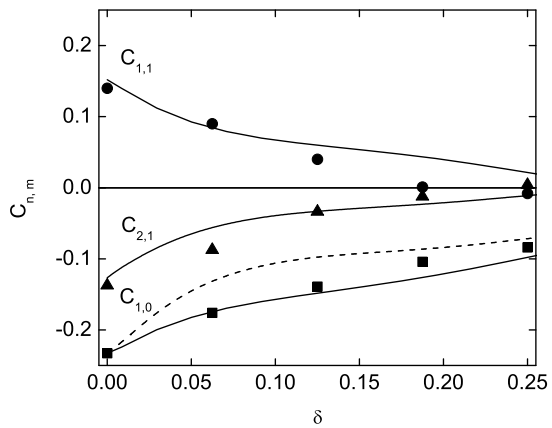


FIG. 1: Spin correlation functions vs doping at $T = 0$ and $J/t = 0.4$ (solid) and the ED data of Ref. [31] (symbols). The function $C_{1,0}$ at $J/t = 0.2$ is plotted by the dashed line.

limit ($\delta = 0$) and their values are taken also at finite δ . For $\delta = 0$ we have $F_{\mathbf{R} \neq 0} = 0$ so that the itinerant contribution to the spectrum (10) vanishes, and $\omega_{\mathbf{q}}$ agrees with the result of Ref. [27], where we have to put $\lambda_2 = 1$, as can be seen from Eq. (A9). At $T = 0$ we fix α_1 and α_2 by the sum rule $C_{0,0} = 1/2$ and, as an input, by the value of the nearest-neighbor correlation function obtained by exact diagonalization (ED), $C_{1,0}^{ED}(\delta = 0) = -0.234$ (Ref. [31]). We get $\alpha_1 = 2.285$ and $\alpha_2 = 2.548$. At finite temperatures we determine $\alpha_1(T)$ and $\alpha_2(T)$ from the sum rule and the ansatz (cf. Refs. [27, 29]) $r(T) \equiv [\alpha_1(T) - 1]/[\alpha_2(T) - 1] = r(0) = 0.830$.

Considering the parameters λ_1 and λ_2 at finite δ , at $T = 0$ we fix them by the sum rule (25) and by the ED value $C_{1,0}^{ED}(\delta = 0.0625; J/t = 0.4) = -0.176$ (Ref. [31]). We get $\lambda_1 = 0.195$ and $\lambda_2 = 0.515$ with $\lambda_1/\lambda_2 = 0.378$. At arbitrary temperatures, doping, and ratios of J/t we determine λ_1 and λ_2 from the sum rule (25) and the ansatz

$$\lambda_1(T, \delta; J/t)/\lambda_2(T, \delta; J/t) = 0.378. \quad (26)$$

In Fig. 1 our results for the doping dependence of the spin correlation functions at $T = 0$ and $J/t = 0.4$ are presented. They show a good agreement with the ED data of Ref. [31]. The different signs of $C_{n,m}$ reflect the AF SRO which gradually decreases with increasing doping and decreasing ratios J/t .

Considering the staggered magnetization $m(\delta)$ at zero temperature which is plotted in Fig. 2, we obtain a strong suppression of LRO with increasing doping due to the spin-hole interaction. In the Heisenberg limit we get $m(0) = 0.303$ which agrees with the value $m(0) = 0.3074$ found in quantum Monte Carlo (QMC) simulations [32]. At the critical doping $\delta_c(J/t)$ we obtain a transition from the LRO phase to a paramagnetic phase with AF SRO. It is remarkable that δ_c is nearly proportional to J/t . This result agrees with that found by the cumulant approach of Ref. [33], where our δ_c values are somewhat lower (e.

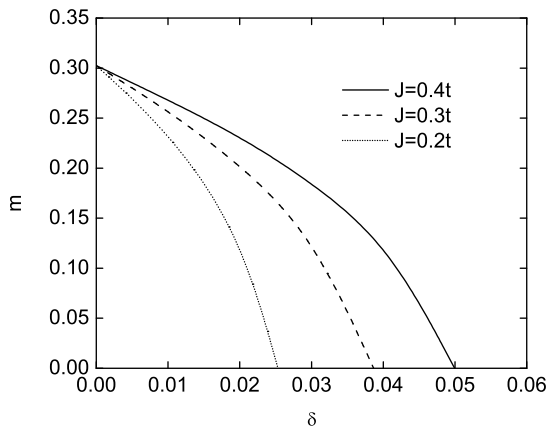


FIG. 2: Staggered magnetization as a function of doping for different values of J/t .

g., in Ref. [33], $\delta_c \simeq 0.06$ for $J/t = 0.4$). Note that the proportionality $\delta_c \propto J/t$ was not found in Ref. [26]. The δ_c values obtained are in qualitative agreement with neutron scattering experiments on $\text{La}_{2-\delta}\text{Sr}_\delta\text{CuO}_4$ (LSCO) which reveal the vanishing of LRO at $\delta_c \simeq 0.02$. [2]

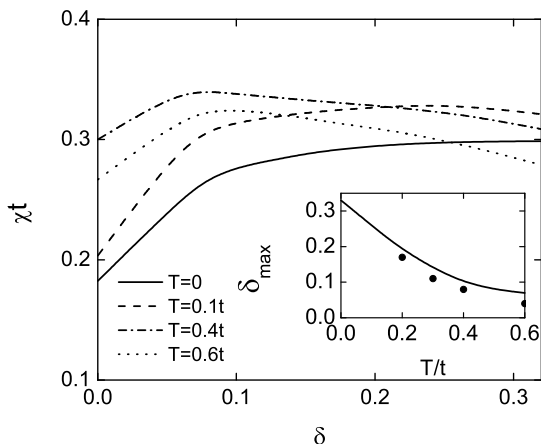


FIG. 3: Uniform static spin susceptibility vs doping at $J/t = 0.3$ for various temperatures. The inset shows the position $\delta_{\max}(T)$ of the maximum in χ vs δ in comparison with the ED data (dots) of Ref. [34].

In Fig. 3 the uniform static spin susceptibility $\chi = (1/2) \lim_{q \rightarrow 0} \chi_{\mathbf{q}}$ at $J/t = 0.3$ is plotted as a function of doping at various temperatures. Within our theory, the increase of $\chi(\delta, T)$ upon doping is caused by the decrease of SRO (cf. Fig. 1), i.e., of the spin stiffness against orientation along a homogeneous external magnetic field. At large enough doping, χ decreases with increasing δ due to the decreasing number of spins. The SRO-induced maximum of χ at $\delta_{\max}(T)$ shifts to lower doping with increasing temperature, since SRO effects are less pronounced at higher T . The doping dependence of χ , especially the maximum at $\delta_{\max}(T)$ (see the inset of Fig. 3), is in accord with the ED results of Ref. [34]. Whereas

the absolute values of χ turn out to be lower than the ED data, the maximum position is in a remarkably good agreement with the ED results. Note that in the spinrotation invariant approach of Ref. [35] for $t \ll J$, the maximum of χ as a function of doping was not reproduced. Our results are in qualitative agreement with experiments on LSCO, where the measured doping dependence of the magnetic susceptibility exhibits a maximum at $\delta_{\max} \simeq 0.25$ over the entire accessible temperature region, $50 \text{ K} \leq T \leq 400 \text{ K}$. [36]

Considering the temperature dependence of $\chi(T, \delta)$ at fixed doping, from Fig. 3 it can be seen that there appears a maximum at $T_{\max}(\delta)$ which shifts to lower temperatures with increasing doping, in qualitative agreement with the ED data [34]. This maximum and the crossover to the high-temperature Curie law $\chi \propto (1 - \delta)/T$ can be understood as a SRO effect, in analogy to the explanation of the doping dependence.

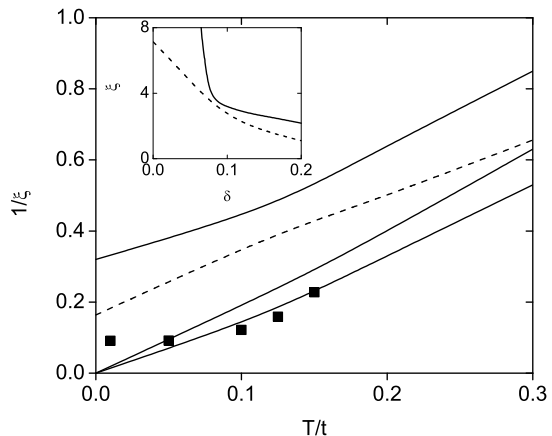


FIG. 4: Inverse AF correlation length vs T at $J/t = 0.4$ (solid lines) for doping $\delta = 0, 0.04, 0.1$, from bottom to top, and at $J/t = 0.2$ (dashed line) for $\delta = 0.04$. The neutron-scattering data on $\text{La}_{2-\delta}\text{Sr}_\delta\text{CuO}_4$ with $\delta = 0.04$ are given by symbols [2]. The inset exhibits the doping dependence of the correlation length at $T = 0$ (solid line) and $T = 0.1t$ (dashed line) at $J/t = 0.4$.

Figure 4 shows the inverse correlation length $\xi^{-1}(T, \delta, J/t)$. The qualitative behavior of ξ in the zero-temperature limit as function of doping and J/t can be easily understood by considering the staggered magnetization at $T = 0$ depicted in Fig. 2. At a given value of J/t and $\delta < \delta_c$, in the limit $T \rightarrow 0$, AF LRO emerges which is connected with the closing of the AF gap, $\omega_{\mathbf{Q}} \rightarrow 0$, and, by Eq. (11), with the divergence of ξ . At zero doping, $\xi^{-1}(T)$ exhibits the known exponential decrease as $T \rightarrow 0$. [27, 29] At $\delta > \delta_c$, the ground state has no AF LRO, i.e., we have $\omega_{\mathbf{Q}} > 0$, and the correlation length saturates at $T \rightarrow 0$. Equally, taking $T = 0$, the transition from the AF LRO phase to a paramagnetic phase with AF SRO at $\delta = \delta_c$ is accompanied by the change $\xi^{-1}(0, \delta < \delta_c, J/t) = 0$ to $\xi^{-1}(0, \delta > \delta_c, J/t) > 0$. Considering the influence of the ratio J/t on the properties of ξ , let us compare the curves

in Fig. 4 for fixed $\delta = 0.04$ and $J/t = 0.4$ and 0.2 . According to Fig. 2, for $J/t = 0.4$ and $J/t = 0.2$ we have $\delta < \delta_c$ and $\delta > \delta_c$, so that $\xi^{-1}(0, \delta, J/t = 0.4) = 0$ and $\xi^{-1}(0, \delta, J/t = 0.2) > 0$, respectively. The weakening of AF correlations (decrease of ξ) with decreasing exchange interaction is in accord with the results for $C_{1.0}$ shown in Fig. 1 for $J/t = 0.4$ and 0.2 . Note that in Ref. [37] a divergence of ξ was found as $T \rightarrow 0$ for arbitrary values of δ , in disagreement with experimental facts. This deficiency may be due to employing various decoupling schemes not used in our theory.

To compare the temperature dependence of $\xi^{-1}(T, \delta)$ with neutron-scattering experiments on LSCO at $T \leq 600$ K, [2] we take $a = 3.79$ Å and $J = 130$ meV and consider the doping $\delta = 0.04$. As can be seen in Fig. 4, we obtain a reasonable agreement with experiments. Concerning the doping dependence of $\xi(\delta, T)$ depicted in the inset of Fig. 4, it can be described approximately by the proportionality $\xi(\delta, T) \propto 1/\sqrt{\delta}$ (dashed line) which agrees with the experimental findings. [2]

B. Spin dynamics

In this section we present results for the spin-fluctuation spectra provided by the imaginary part of the DSS $\chi''(\mathbf{q}, \omega)$, Eq. (7), where we neglect the real part of the self-energy $\Sigma'(\mathbf{q}, \omega)$ (cf. Ref. [28]). The damping of spin fluctuations $\Gamma(\mathbf{q}, \omega)$ is determined by the imaginary part of the self-energy, $\Gamma(\mathbf{q}, \omega) = -(1/2)\Sigma''(\mathbf{q}, \omega)$, considered in Sec. II.C. Here we mainly consider the damping at $\omega = \omega_{\mathbf{q}}$, $\Gamma_{\mathbf{q}} = \Gamma(\mathbf{q}, \omega_{\mathbf{q}})$. It turns out that the major contributions to the damping are given by the diagonal terms $\Sigma''_j(\mathbf{q}, \omega)$, Eq. (15), and $\Sigma''_t(\mathbf{q}, \omega)$, Eq. (17), while the interference terms, such as $\Sigma''_{j_t, j_t}(\mathbf{q}, \omega)$, Eq. (B4), appear to be much smaller and may be neglected. That is, the damping $\Gamma_{\mathbf{q}}$ is the sum of the spin-spin scattering contribution $\Gamma_{J, \mathbf{q}} = -(1/2)\Sigma''_j(\mathbf{q}, \omega_{\mathbf{q}})$ and the spin-hole scattering contribution $\Gamma_{t, \mathbf{q}} = -(1/2)\Sigma''_t(\mathbf{q}, \omega_{\mathbf{q}})$, $\Gamma_{\mathbf{q}} = \Gamma_{J, \mathbf{q}} + \Gamma_{t, \mathbf{q}}$. Note that in Refs. [20] and [21] the partition of the damping into a spin-exchange contribution and a fermionic contribution was suggested from the ED data. The numerical calculations of $\Sigma''(\mathbf{q}, \omega)$ are performed for the exchange interaction $J = 0.3t$, the value which is usually used in numerical simulations. This affords us to compare our analytical results with finite cluster calculations and to check the reliability of our approximations.

Let us first consider the Heisenberg limit $\delta = 0$. Figure 5 shows the spin-excitation spectrum $\omega_{\mathbf{q}}$, Eq. (10), and the damping $\Gamma_{\mathbf{q}} = \Gamma_{J, \mathbf{q}}$. The results are similar to those obtained in Ref. [28]. In the spin-wave region, at $q\xi \gg 1$, we get well-defined quasiparticles with $\Gamma_{\mathbf{q}} \ll \omega_{\mathbf{q}}$. For example, for $\mathbf{q} = \pi(1/2, 1/2)$ and $T = 0.35J$ we have $q \gg \xi^{-1} \simeq 0.1$ (see Fig. 4) and $\Gamma_{\mathbf{q}}/\omega_{\mathbf{q}} \simeq 0.1$. Well-defined spin excitations for the two-dimensional Heisenberg model have been found by several authors (for a review see Ref. [4]). In particular, as shown in Ref. [38], if $T \rightarrow 0$ and $q \rightarrow 0$ with the restriction $q\xi \gg 1$, the ratio

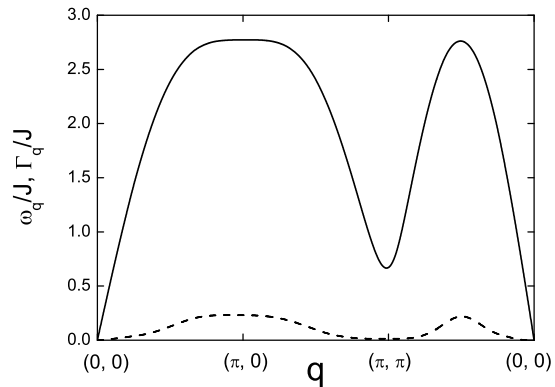


FIG. 5: Spectrum $\omega_{\mathbf{q}}$ (solid line) and damping $\Gamma_{\mathbf{q}}$ (dashed line) in the Heisenberg limit, $\delta = 0$, at $T = 0.35J$.

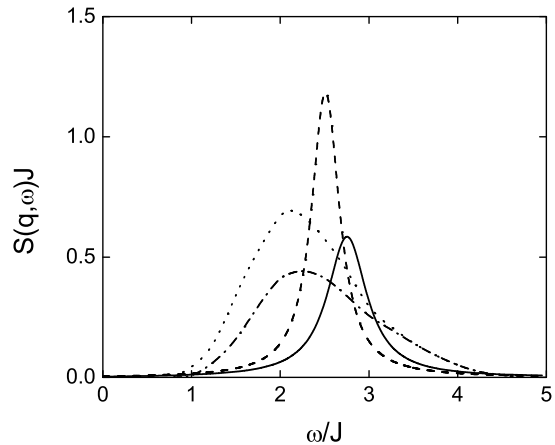


FIG. 6: Dynamic structure factor $S(\mathbf{q}, \omega)$ in the Heisenberg limit, $\delta = 0$, at $T = 0.38J$ for wave vectors: $\mathbf{q}_1 = \pi(1/2, 1/2)$ (solid line) and $\mathbf{q}_2 = \pi(5/8, 5/8)$ (dashed line) in comparison with the QMC results of Ref. [39] for \mathbf{q}_1 (dashed-dotted line) and for \mathbf{q}_2 (dotted line).

of the damping to the spin-wave excitation energy tends to zero: $\Gamma_{J, \mathbf{q}}/\omega_{\mathbf{q}} \rightarrow 0$.

To compare our results for the damping with the QMC data of Ref. [39], we have considered the linewidth $\Lambda_{\mathbf{q}}$ of the relaxation function $F(\mathbf{q}, \omega) = 4[\beta\omega\chi_{\mathbf{q}}]^{-1}\chi''(\mathbf{q}, \omega)$ at $T = 0.35J$, where $\Lambda_{\mathbf{q}} \simeq 2\Gamma_{\mathbf{q}}$ (Ref. [28]), and have found a good agreement. For a further comparison with the QMC data we calculate the dynamic structure factor $S(\mathbf{q}, \omega) = [1 - \exp(-\beta\omega)]^{-1}\chi''(\mathbf{q}, \omega)$. In Fig. 6 our results at $T = 0.38J$ and for two wave vectors in the spin-wave region are plotted. The peaks in $S(\mathbf{q}, \omega)$, occurring nearly at $\omega_{\mathbf{q}}$ (cf. Fig. 5), reveal well-defined spin excitations. Comparing the peak heights with the QMC values, we get a better agreement than it was found in Ref. [28]. This may be ascribed to Eq. (15) which corrects the result of Ref. [28] by the appearance of the additional term $\Gamma_{\mathbf{q}_1\mathbf{q}_2\mathbf{q}_3}\Gamma_{\mathbf{q}_2\mathbf{q}_1\mathbf{q}_3}$ that cannot be written as a square of the vertex $\Gamma_{\mathbf{q}_1\mathbf{q}_2\mathbf{q}_3}$.

For non-zero doping the spin-hole scattering contri-

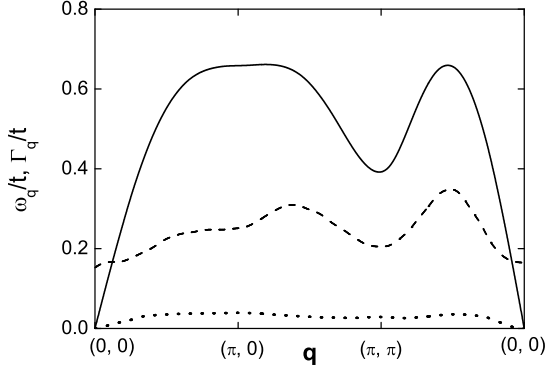


FIG. 7: Spectrum $\omega_{\mathbf{q}}$ (solid line), and damping $\Gamma_{J,\mathbf{q}}$ (dotted line) and $\Gamma_{t,\mathbf{q}}$ (dashed line) at $T = 0.15t$ and $\delta = 0.1$.

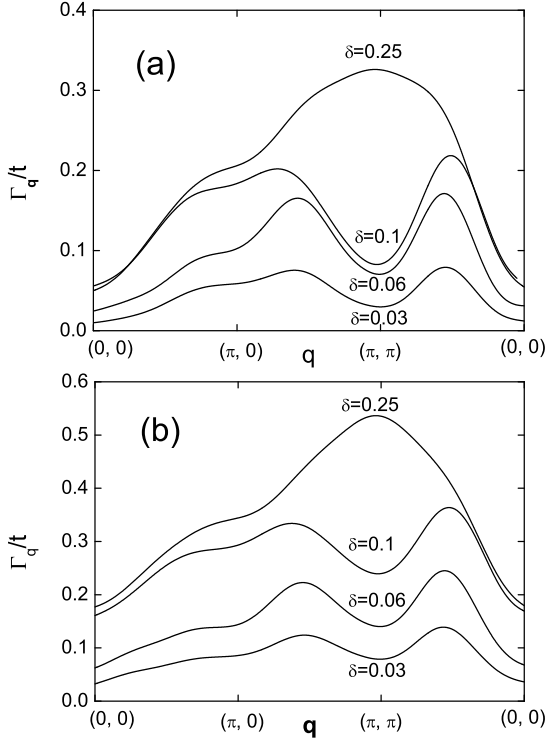


FIG. 8: Doping dependence of damping $\Gamma_{\mathbf{q}}$ at $T = 0.1t$ (a) and $T = 0.15t$ (b).

bution $\Sigma''_t(\mathbf{q}, \omega)$, Eq. (17), increases rapidly with doping and temperature and already at moderate hole concentration far exceeds the spin-spin scattering contribution $\Sigma''_J(\mathbf{q}, \omega)$, Eq. (15), as demonstrated in Figs. 7 and 8. Depending on \mathbf{q} , doping, and temperature, the spin excitations may have a different character and dynamics. In particular, for the spin-spin scattering contribution $\Sigma''_J(\mathbf{q}, \omega)$ we observe, in the long-wavelength limit, $\lim_{\mathbf{q} \rightarrow 0} \Gamma_{J,\mathbf{q}} = 0$, as in the case of the Heisenberg model shown in Fig. 5. Contrary to this behavior, the damping $\Gamma_{t,\mathbf{q}}$, induced by the spin-hole scattering, is finite in this limit, both taking Eq. (17) and Eq. (19). The different behavior of $\Gamma_{J,\mathbf{q}}$ and $\Gamma_{t,\mathbf{q}}$ may

be explained by the different \mathbf{q} -dependence of the spectral functions entering Eqs. (15) and (17). Whereas for spin excitations the spectral function is proportional to $m(\mathbf{q})/\omega_{\mathbf{q}} \sim q$ for $q \rightarrow 0$ (see Eq. (20)), for electrons it is finite in this limit (see Eq. (22)). Therefore, in the limit of $\mathbf{q} = \mathbf{q}_1 + \mathbf{q}_2 + \mathbf{q}_3 = 0$, for the spin-spin scattering the product $m(\mathbf{q}_1)m(\mathbf{q}_2)m(\mathbf{q}_3)/\omega_{\mathbf{q}_1}\omega_{\mathbf{q}_2}\omega_{\mathbf{q}_3}$ gives a vanishingly small contribution to the integrals over $\mathbf{q}_1, \mathbf{q}_2$ in $\Sigma''_J(\mathbf{q}, \omega)$, Eq. (15), while in the spin-hole self-energy (17) there is no such a small factor. The physical meaning of the finite damping $\Gamma_{t,\mathbf{q}}$ at $q = 0$ can be explained similarly to that of the finite electrical conductivity in the low-frequency limit, which is in fact a response function determining the damping of charge fluctuations at $\mathbf{q} = 0$. As is well known, the relaxation rate for the conductivity at zero frequency, i.e., the inverse resistivity, is finite, if one takes into account momentum relaxation of electron-hole pairs on phonons.

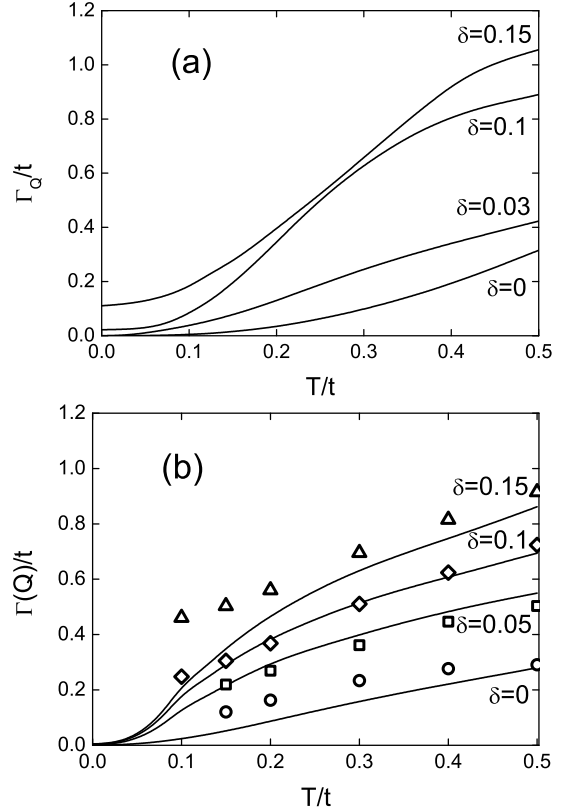


FIG. 9: Damping $\Gamma_{\mathbf{Q}} = -(1/2)\Sigma''(\mathbf{Q}, \omega = \omega_{\mathbf{Q}})$ (a) and low energy damping $\Gamma(\mathbf{Q}) = -(1/2)\Sigma''(\mathbf{Q}, \omega = 0)$ (b) as functions of temperature and doping in comparison with the ED data of Ref. [21] (symbols).

To discuss the temperature and doping dependence of the damping (see Fig. 8) in more detail, we choose $\mathbf{q} = \mathbf{Q}$ and consider the damping $\Gamma_{\mathbf{Q}} = -(1/2)\Sigma''(\mathbf{Q}, \omega_{\mathbf{Q}})$ as function of T and δ that is plotted in Fig. 9 (a). In the zero-temperature limit and for $\delta < \delta_c$, where there is AF LRO (see Fig. 2), it can be shown analytically that $\Gamma_{\mathbf{Q}}(T = 0, \delta < \delta_c) = 0$. That is, in the LRO phase we

get well-defined spin waves. The vanishing of $\Gamma_{\mathbf{Q}}$ may be explained as follows. Spin excitations at $T = 0$ can decay into particle-hole excitations with a positive energy ω only to satisfy the energy conservation law. Here, $\omega = \omega_{\mathbf{Q}} = 0$ for $\delta < \delta_c$ so that we have no damping. On the other hand, at $T = 0$ and $\delta > \delta_c$, there is no LRO and $\omega_{\mathbf{Q}} > 0$ which results in $\Gamma_{\mathbf{Q}}(T = 0, \delta > \delta_c) > 0$ (see Fig. 9 (a) for $\delta = 0.1$ and 0.15). With increasing temperature and doping the damping increases as expected. To compare our results with the data of Ref. [21], in Fig. 9 (b) the temperature dependence of the low-energy damping $\Gamma(\mathbf{Q}) = -(1/2)\Sigma''(\mathbf{Q}, \omega = 0)$ for various doping is shown. In Ref. [21] the function $\gamma(\mathbf{Q}) = 2\Gamma(\mathbf{Q})$ was extracted from the finite- T Lanczos data for the spectral function $\chi''(q, \omega)$ using a simplified ansatz for the spin-excitation spectrum, $\omega_{\mathbf{q}} \propto ((\mathbf{q} - \mathbf{Q})^2 + \kappa^2)$ with $\kappa = \xi^{-1}$ taken as a temperature-independent parameter, whereas our theory allows a direct microscopic calculation of $\Gamma(\mathbf{Q})$. In the high-temperature region a remarkably good agreement is found. In the low-temperature region, which is not accessible by the finite- T Lanczos method, the ED results were extrapolated to $T = 0$ with a finite value of $\Gamma(\mathbf{Q}; T = 0, \delta > 0)$. This is in contrast to our result $\Gamma(\mathbf{Q}; T = 0, \delta) = 0$ (cf. Fig. 9 (b)) which agrees with $\Gamma_{\mathbf{Q}}(T = 0, \delta < \delta_c) = 0$ (cf. Fig. 9 (a)), because both quantities are calculated for $\omega = 0$, and which may be understood as explained above.

As illustrated in Fig. 8 and Fig. 9, at low enough doping and temperature, i.e., at small enough $\Gamma_{t, \mathbf{q}}$, we may observe well-defined high-energy spin-wave-like excitations with $q, k \gg 1/\xi$ ($k = |\mathbf{q} - \mathbf{Q}|$) and $\Gamma_{\mathbf{q}} \ll \omega_{\mathbf{q}}$ propagating in AF SRO. Considering, for example, spin excitations with $\mathbf{q} = (\pi, 0)$ at $\delta = 0.1$ and $T = 0.15t$, we have $q\xi = 5.8$ with $\xi = 1.85$ taken from Fig. 4, $\omega_{\mathbf{q}} = 0.66t$, and $\Gamma_{\mathbf{q}} = 0.27t$ (see Figs. 7 and 8 (b)). That is, in this case we have strongly damped spin waves.

To discuss quantitatively the spectral function $\chi''(\mathbf{q}, \omega)$ shown in Figs. 10 and 11, in particular the position of its maximum at ω_m , we first simplify Eq. (7). By numerical evaluations, we have found that the imaginary part of the self-energy only weakly depends on frequency, which qualitatively agrees with the results of Ref. [21]. Therefore, we put $-\Sigma''(\mathbf{q}, \omega) = \eta_{\mathbf{q}} \simeq 2\Gamma_{\mathbf{q}}$. Then, by Eq. (7) we get the resonance form

$$\chi''(\mathbf{q}, \omega) = m(\mathbf{q}) \frac{\eta_{\mathbf{q}} \omega}{(\omega^2 - \omega_{\mathbf{q}}^2)^2 + \eta_{\mathbf{q}}^2 \omega^2}, \quad (27)$$

which has a maximum at ω_m^R given by

$$\omega_m^R = \frac{1}{\sqrt{6}} \{2\omega_{\mathbf{q}}^2 - \eta_{\mathbf{q}}^2 + [12\omega_{\mathbf{q}}^4 + (2\omega_{\mathbf{q}}^2 - \eta_{\mathbf{q}}^2)^2]^{1/2}\}^{1/2}, \quad (28)$$

where $\lim_{\eta \rightarrow 0} \omega_m^R = \omega_{\mathbf{q}}$.

Let us consider the region of low-frequency overdamped spin-fluctuation modes playing an important role in the normal phase of the cuprate superconductors, i.e., $\omega < \omega_{\mathbf{q}} \ll \eta_{\mathbf{q}}$. Expanding Eq. (27) with respect to

$\omega/\eta_{\mathbf{q}} < \omega_{\mathbf{q}}/\eta_{\mathbf{q}} \ll 1$ and using Eq. (3) we get

$$\chi''(\mathbf{q}, \omega) = \chi_{\mathbf{q}} \tilde{\Gamma}_{\mathbf{q}} \frac{\omega}{\omega^2 + \tilde{\Gamma}_{\mathbf{q}}^2}; \quad \tilde{\Gamma}_{\mathbf{q}} = \frac{\omega_{\mathbf{q}}^2}{\eta_{\mathbf{q}}}, \quad (29)$$

where $\tilde{\Gamma}_{\mathbf{q}}$ is the spin-fluctuation excitation energy. Contrary to Ref. [21], where a similar expression was derived, we do not use an ansatz for the spin-excitation spectrum $\omega_{\mathbf{q}}$ (see above), but calculate it microscopically by the GMFA [see Eq. (10)]. The Lorentzian (29) has a maximum at $\omega_m^S = \tilde{\Gamma}_{\mathbf{q}}$, which may be also obtained from the expansion of Eq. (28) with respect to $(\omega_{\mathbf{q}}/\eta_{\mathbf{q}})^2$. The overdamped form corresponds to the susceptibility $\chi(\mathbf{q}, \omega) = \chi_{\mathbf{q}} \tilde{\Gamma}_{\mathbf{q}} (\tilde{\Gamma}_{\mathbf{q}} - i\omega)^{-1}$ and, as a phenomenological ansatz, has been frequently invoked in the study of cuprates, e.g., in the calculation of the normal-state spin-fluctuation conductivity. [40]

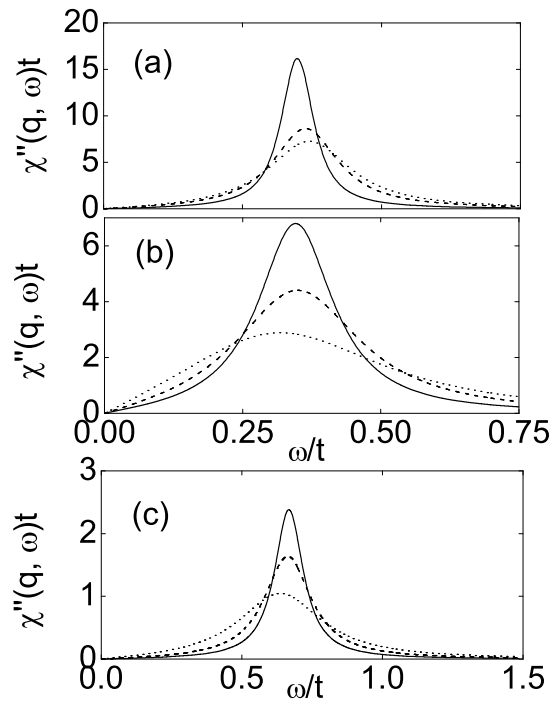


FIG. 10: Spectral function $\chi''(\mathbf{q}, \omega)$ for $\mathbf{q} = \mathbf{Q} = (\pi, \pi)$ at $T = 0.1t$ (a) and $T = 0.15t$ (b) for $\delta = 0.03$ (solid line), $\delta = 0.06$ (dashed line), and $\delta = 0.1$ (dotted line), and for $\mathbf{q} = (\pi, 0)$ at $T = 0.1t$ (c) [note the change in the energy scale].

To exemplify the spin dynamics in different regions, we first consider spin waves with $\mathbf{q} = (\pi, 0)$ at $\delta = 0.1$ and $T = 0.15t$ (see above). We get (see Fig. 11) $\omega_m = 0.59t \simeq \omega_m^R = 0.60t$ and $\omega_m^S = 0.81t$. That is, we find those excitations to have a resonance character. On the other hand, the ED data of Ref. [21] yield evidence for an overdoped spin dynamics. This difference may be due to a slight underestimation of the damping in our theory, which can be also seen in the more pronounced peaks of the dynamic structure factor at $\delta = 0$

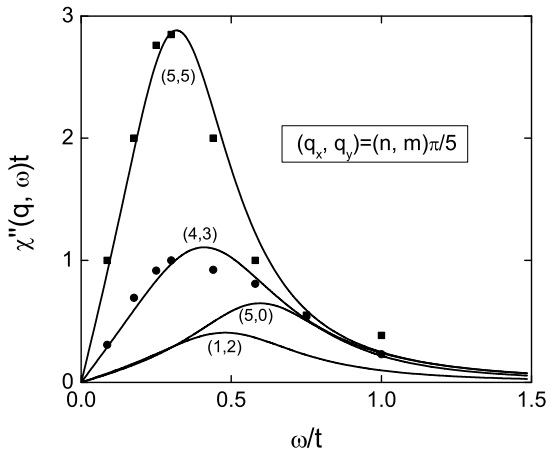


FIG. 11: Spectral function $\chi''(\mathbf{q}, \omega)$ for various wave vectors at $T = 0.15t$ and $\delta = 0.1$ in comparison with ED data (filled symbols, Ref. [21]).

(see Fig. 6) as compared with the QMC data. As seen in Fig. 10 (c), with increasing δ the maximum in $\chi''(\mathbf{q}, \omega)$ with $\mathbf{q} = (\pi, 0)$ is shifted to lower frequencies, in qualitative agreement with the theory of Ref. [18].

Next we consider the spectral function at $\mathbf{q} = \mathbf{Q}$. At very low doping, e.g., $\delta = 0.03$, and low enough temperature the damping $\Gamma_{\mathbf{Q}}$ is very small (see Fig. 8 and Fig. 9 (a)), where $\Gamma_{\mathbf{Q}} \ll \omega_{\mathbf{Q}}$. In this case we observe underdamped spin modes characterized by sharp resonance peaks in $\chi''(\mathbf{Q}, \omega)$, as seen in Fig. 10 (a), (b). With increasing doping those modes evolve into overdamped (relaxation-type) spin-fluctuation modes (AF paramagnons) described by the broad spectrum (29). For example, considering the AF mode at $\delta = 0.1$ and $T = 0.15t$ (see Figs. 7, 8 (b), 10 (b), and 11), we have $\omega_{\mathbf{Q}} = 0.4t$, $\Gamma_{\mathbf{Q}} = 0.24t$, and $\omega_m = 0.32t \simeq \omega_m^S = 0.33t$. That is, the spectrum of this mode may be well described by the overdamped form (29). As seen in Fig. 11, our spin-fluctuation spectrum is in a remarkably good agreement with the ED data of Ref. [21]. Let us consider the shift of the maximum in $\chi''(\mathbf{Q}, \omega)$ at ω_m with increasing doping at fixed temperature. As can be seen from Fig. 10 (a), (b), at low (high) temperatures, ω_m slightly increases (decreases) with doping, which results from the doping dependence of $\omega_{\mathbf{q}}$ and $\Gamma_{\mathbf{q}}$. The increase of ω_m with δ at low T is in qualitative agreement with the findings of Ref. [18] ($T = 0.02t$) and with experiments.

In Fig. 12 the dynamic structure factor $S(\mathbf{q}, \omega)$, resulting from the spectral function shown in Fig. 11, is plotted. At $\omega = 0$, by Eq. (7), we have $S(\mathbf{q}, 0) = T\chi_{\mathbf{q}}\Sigma''(\mathbf{q}, 0)/\omega_{\mathbf{q}}^2$, and for overdamped modes [Eq. (29)] we get $S(\mathbf{q}, 0) = T\chi_{\mathbf{q}}/\tilde{\Gamma}_{\mathbf{q}}$. The shape of $S(\mathbf{q}, \omega)$ for paramagnons is in a marked contrast to that for spin waves (compare also with Fig. 6).

Finally, we present results for the local susceptibility

$$\chi_L''(\omega) = \frac{1}{N} \sum_{\mathbf{q}} \chi''(\mathbf{q}, \omega), \quad (30)$$

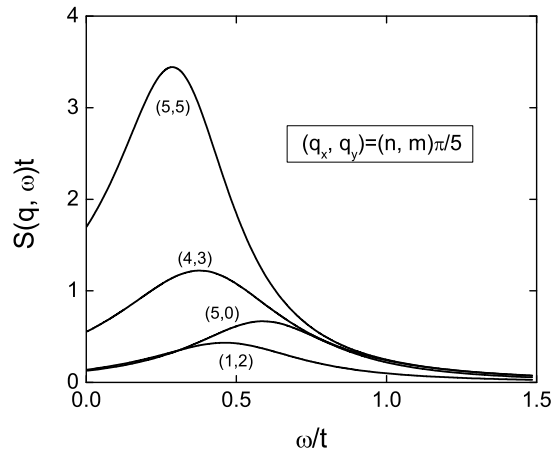


FIG. 12: Dynamic structure factor $S(\mathbf{q}, \omega)$ at $T = 0.15t$ and $\delta = 0.1$ for various wave vectors.

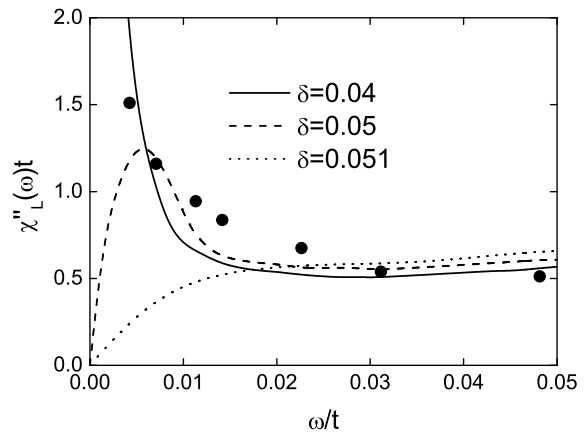


FIG. 13: Local spin susceptibility $\chi_L''(\omega)$ at $T = 0$ and small doping. The intensity scaled experimental data on $\text{La}_{1.96}\text{Sr}_{0.04}\text{CuO}_4$ at $T = 10$ K are shown by dots [41], where $t = 420$ meV is taken.

by using the data for $\chi''(\mathbf{q}, \omega)$, Eq. (7). In Fig. 13 the local susceptibility at $T = 0$ and small doping, $\delta = 0.04 - 0.051$, is shown. In the neighborhood of the AF phase transition at $T = 0$ and $\delta = \delta_c = 0.037$ (see Fig. 2; $\omega_{\mathbf{Q}} = 0$), the spin excitations with $\mathbf{q} \simeq \mathbf{Q}$ are weakly damped (see Fig. 9 (a)). Therefore, at sufficiently low δ , the local susceptibility, which is just the density of states (DOS) for spin-fluctuations, reveals a resonance maximum at a frequency being close to $\omega_{\mathbf{Q}}$ with a high DOS (see Fig. 13 at $\delta = 0.05$). Because $\omega_{\mathbf{Q}}$ and $\Gamma_{\mathbf{Q}}$ decrease with decreasing δ , the maximum shifts to lower frequencies and becomes very sharp (in Fig. 13 at $\delta = 0.04$, only the upturn with decreasing frequency is seen). On the other hand, with increasing doping the damping becomes large enough to wash away the maximum (cf. Fig. 13). Note that we obtain, in addition to the low-energy maximum, a broad maximum in $\chi_L''(\omega)$ at the maximum energy of spin excitations, $\omega \sim 2J = 0.6t$ (cf. Fig. 5). This feature was not found in Ref. [21], since a

simplified spin-excitation spectrum $\omega_{\mathbf{q}}$ was used.

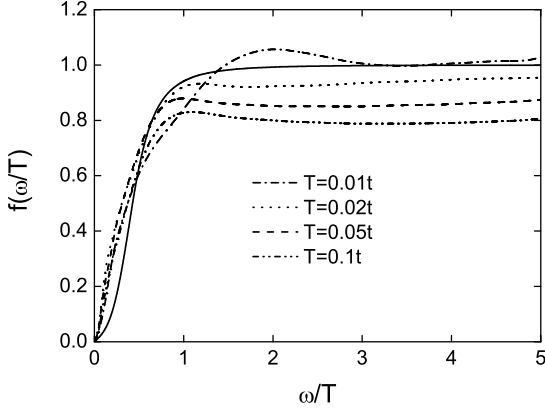


FIG. 14: Scaling function $f(\omega/T)$ for various temperatures at doping $\delta = 0.04$. The solid line is the scaling function found in the neutron-scattering experiments on $\text{La}_{1.96}\text{Sr}_{0.04}\text{CuO}_4$ (Ref. [41]) and given by Eq. (31).

The pronounced upturn behavior is observed in neutron-scattering experiments on lightly doped cuprate compounds at low energies and temperatures (see, e.g., Refs. [41] and [42]). We get a reasonable agreement with experimental data for $\text{La}_{1.96}\text{Sr}_{0.04}\text{CuO}_4$ ($\omega < 50$ meV) [41], if we take the energy scale $t = 420$ meV (see Fig. 13), which is the standard value of $t \simeq 400$ meV in the t - J model for cuprates. A much better agreement with the data in Ref. [41] can be obtained at the finite temperature $T = 0.01t$ but for the energy scale $t = 1.1$ eV. A qualitatively similar behavior has been found in Ref. [21] within a semi-phenomenological theory, where the agreement with experiment was achieved by the choice $t \sim 0.1$ eV.

Figure 14 shows the scaling function $f(\omega/T) = \chi_L''(\omega, T)/\chi_L''(\omega, T = 0)$. The scaling behavior is in a remarkable agreement with the data of the neutron-scattering experiments on $\text{La}_{1.96}\text{Sr}_{0.04}\text{CuO}_4$ (Ref. [41]) which is shown by the solid line and described by the function

$$f\left(\frac{\omega}{T}\right) = \frac{2}{\pi} \arctan \left[a_1 \left(\frac{\omega}{T}\right) + a_2 \left(\frac{\omega}{T}\right)^3 \right], \quad (31)$$

with $a_1 = 0.43$ and $a_2 = 10.5$. A similar scaling was observed in the underdoped $\text{YBa}_2\text{Cu}_3\text{O}_{6.35}$ with the parameters $a_1 = 0.9$ and $a_2 = 2.8$ (Ref. [42]). Our results may be well approximated by the scaling function (31) with $a_1 = 3$, but without the $(\omega/T)^3$ term, $a_2 = 0$, that gives a nonlinear behavior at low values of $(\omega/T) \ll 1$. The weak non-monotonous behavior of our scaling function at $T = 0.01t$ results from the appearance of a flat maximum in $\chi_L''(\omega, T)$ (see above). Note that in Ref. [21] the same scaling function (31) was found with $a_1 = 1.2$, $a_2 = 0$, that results in the saturation $f(\omega/T) \rightarrow 1$ at higher values of $(\omega/T) \gtrsim 2$ and in strong deviations from the experiments on LSCO reported in Ref. [41], but yields a good fit to experiments on Zn-substituted $\text{YBa}_2\text{Cu}_3\text{O}_{6.6}$ [43].

This variation of the scaling function may be explained by different values of doping and of the corresponding parameters determining the scaling behavior (e.g., the AF correlation length ξ , Ref. [21]).

To sum up, our studies of the DSS show a crossover from well-defined spin-wave-like excitations at low doping and temperatures to relaxation-type spin-fluctuation excitations with increasing hole doping, which is in agreement with inelastic neutron-scattering experiments and numerical simulations for finite clusters. Moreover, we observe a remarkable agreement of the scaling function with the data of neutron-scattering experiments on LSCO. [41]

IV. CONCLUSION

The relaxation-function theory for the DSS in the t - J model in terms of Hubbard operators is formulated. By using a spin-rotation-invariant theory for the DSS derived by us in Ref. [25], we calculate the static properties in the GMFA similarly to Ref. [26] and the spin-fluctuation spectra. The mode-coupling approximation for the force-force correlation functions, which take into account both the exchange and kinetic contributions, was used. For the undoped case described by the Heisenberg model our results are similar to those in Ref. [28] and for finite doping they show a reasonable agreement with available ED data and neutron scattering experiments.

Contrary to the previous studies based on the memory-function method in Refs. [18] – [21], we have taken into account all contributions to the spin-excitation spectrum $\omega_{\mathbf{q}}$ in the GMFA and to the self-energy $\Sigma(\mathbf{q}, \omega)$ and thoroughly analyzed their temperature and doping dependence. In particular, we have found that the contribution from the hole-hopping term $\propto t^2$ in the spectrum $\omega_{\mathbf{q}}$, Eq. (10), is large even in the underdoped region, $\delta \lesssim 0.1$, and results in a rapidly increasing with doping gap $\omega_{\mathbf{Q}}$ at the AF wave vector \mathbf{Q} . This increase is much larger than in the calculations in Ref. [18], where the t^2 contribution has not been considered. We have also shown that the largest contribution to the self-energy $\Sigma(\mathbf{q}, \omega)$ comes from the hole-hopping term $\Sigma_t''(\mathbf{q}, \omega) \propto t^4$, Eq. (17), at finite doping (see Fig. 7). This is in accord with Ref. [20], but contrary to the approximation in Refs. [18], [19], and [22], where only the mixed contribution $\Sigma_{Jt, Jt}''(\mathbf{q}, \omega) \propto J^2 t^2$ has been taken into account. The latter approximation should strongly underestimate the damping of spin excitations at finite doping. In our calculations of $\Sigma_t''(\mathbf{q}, \omega)$ we have also considered explicitly a contribution from spin excitations in the self-energy (see Eq. (17)), while in Refs. [20] and [22] this contribution has been considered in some kind of static or mean-field-type approximations.

A comparison of the DSS derived within the memory-function approach, Eq. (7), with the RPA form $\chi(\mathbf{q}, \omega) = \chi_0(\mathbf{q}, \omega)/[1 - g_{\mathbf{q}}\chi_0(\mathbf{q}, \omega)]$ (see, e.g., Ref. [5]) has shown that the RPA expression provides reasonable results at large doping, while in the underdoped region the RPA

formula fails to describe spin-wave-like excitations. [24] Whereas the damping of spin excitations in Eq. (7) at low doping is quite small, e.g. $\Gamma_{\mathbf{q}} \sim 0.2t$ at $\delta = 0.1$ (see Fig. 7), within the RPA it is much larger, $\Gamma \sim t$. This results in overdamped spin dynamics described by Eq. (29) even in the underdoped region. Thus, we conclude that the relaxation-function approach is a reliable theory for studying the spin dynamics in a broad region of doping and temperatures.

In this paper we have not performed a fully self-consistent calculation of the electronic and spin-fluctuation spectra by evaluating the spin correlation functions (21) in the GMFA and the electron correlation functions (23) in the Hubbard I approximation. As was shown in Ref. [44], static AF spin correlations and self-energy effects result in a strong renormalization of the electronic spectra and should be taken into account in a consistent theory. This generalization will be considered in a subsequent publication. The theory will be also formulated for the superconducting state by introducing matrix electronic GF with normal and anomalous components as given in Ref. [44].

Acknowledgments

The authors thank Ilya Eremin for valuable discussions. Partial financial support by the Heisenberg-Landau Program of JINR is acknowledged. One of the authors (N.P.) is grateful to the MIPKKS, Dresden, for the hospitality during his stay at the Institute, where a part of the present work has been done.

APPENDIX A: DECOUPLING PROCEDURE

To calculate the correlation function $(-\tilde{S}_i^+, S_l^-)$ in Eq. (8) we consider the equation

$$-\tilde{S}_i^+ = [[S_i^+, (H_t + H_J)], (H_t + H_J)] \equiv \sum_{\alpha} F_i^{\alpha}, \quad (\text{A1})$$

where H_t and H_J are the hopping and the exchange parts of the Hamiltonian (1) and $\alpha = tt, tJ, Jt, JJ$. Here we have

$$F_i^{tt} = \sum_{j,n} t_{ij} \left\{ t_{jn} [H_{ijn}^- + H_{nji}^+] - (i \iff j) \right\}, \quad (\text{A2})$$

$$F_i^{JJ} = \frac{1}{4} \sum_{j,n} J_{ij} \left\{ J_{jn} [2P_{ijn} + \Pi_{ijn}] - (i \iff j) \right\}, \quad (\text{A3})$$

$$F_i^{Jt} = [[S_i^+, H_J], H_t], \quad F_i^{tJ} = [[S_i^+, H_t], H_J], \quad (\text{A4})$$

where

$$H_{ijn}^{\sigma} = X_i^{\sigma 0} X_j^{+ -} X_n^{0 \sigma} + X_i^{+ 0} (X_j^{0 0} + X_j^{\sigma \sigma}) X_n^{0 -}, \quad (\text{A5})$$

$$\begin{aligned} P_{ijn} &= S_i^z S_j^z S_n^+ + S_n^+ S_i^z S_j^z \\ &- S_i^z S_j^+ S_n^z - S_n^z S_i^z S_j^+, \end{aligned} \quad (\text{A6})$$

$$\begin{aligned} \Pi_{ijn} &= S_i^+ S_j^- S_n^+ + S_n^+ S_i^+ S_j^- \\ &- S_i^+ S_j^+ S_n^- - S_n^- S_i^+ S_j^+. \end{aligned} \quad (\text{A7})$$

Explicit expressions for F_i^{tJ}, F_i^{Jt} are given in Ref. [25].

To evaluate the corresponding multiparticle correlation functions in $(-\tilde{S}_{\mathbf{q}}^+, S_{-\mathbf{q}}^-)$ we perform the following decoupling procedure similar to that proposed in Refs. [26, 28, 29, 35] preserving the local correlations. The correlation functions from H_{ijn}^{σ} are decoupled as

$$(X_i^{\sigma 0} X_j^{+ -} X_n^{0 \sigma}, S_l^-) = \lambda_1 \langle X_i^{\sigma 0} X_n^{0 \sigma} \rangle (S_j^+, S_l^-), \quad (\text{A8})$$

where, for $n = i$, $\langle X_i^{\sigma 0} X_i^{0 \sigma} \rangle = \langle X_i^{\sigma \sigma} \rangle = n/2$ and the second term of H_{ijn}^{σ} with $n \neq i$ is neglected (cf. Ref. [26]). Decoupling the correlation functions from $\Pi_{ijn=i}$ and $P_{ij,n=i}$ we introduce the parameter λ_2 :

$$\begin{aligned} (\Pi_{iji}, S_l^-) &= -([X_i^{++} + X_i^{--}] S_j^+, S_l^-) \\ &= -\lambda_2 \langle [X_i^{++} + X_i^{--}] \rangle (S_j^+, S_l^-); \\ (P_{iji}, S_l^-) &= -(1/2) ([X_i^{++} + X_i^{--}] S_j^+, S_l^-) \\ &= -\lambda_2 (1/2) \langle [X_i^{++} + X_i^{--}] \rangle (S_j^+, S_l^-), \end{aligned} \quad (\text{A9})$$

where we used the equations: $S_i^+ S_i^- = X_i^{++}, S_i^z S_i^+ + S_i^+ S_i^z = 0$, and $(S_i^z)^2 = (1/4)(X_i^{++} + X_i^{--})$. Here we take $\lambda_2 \neq \lambda_1$, in contrast to the approach of Refs. [26, 45], $\lambda_2 = \lambda_1$. In the Heisenberg limit $\delta = 0$ we have $X_i^{++} + X_i^{--} \equiv 1$ so that $\lambda_2 = 1$. The parameters λ_1, λ_2 describe the renormalization of the vertex for spin scattering on charge fluctuations.

Considering the correlation functions from $\Pi_{ijn \neq i}$ and $P_{ijn \neq i}$, where $\{i, j, n\}$ forms a nearest-neighbor sequence, we apply the decoupling scheme used in Refs. [26, 28, 29]:

$$\begin{aligned} (S_i^+ S_j^+ S_n^-, S_l^-) &= \alpha_1 \langle S_j^+ S_n^- \rangle (S_i^+, S_l^-) \\ &+ \alpha_2 \langle S_i^+ S_n^- \rangle (S_j^+, S_l^-). \end{aligned} \quad (\text{A10})$$

Here, the parameters α_1 and α_2 are attached to nearest-neighbor and further-distant correlation functions, respectively, and describe the renormalization of the vertex for spin-spin scattering. The determination of all parameters is considered in Sec. III.A.

Calculating the spin-excitation spectrum and the static susceptibility (3) with Eq. (8) we may take into account only the diagonal contributions (A2) and (A3) and omit the mixed contributions corresponding to F_i^{Jt} and F_i^{tJ} in Eq. (A4) according to the following reasoning. The mixed contribution of the type (F_i^{Jt}, S_l^-) in the GMFA is proportional to the difference of the correlation functions of the form $\langle X_i^{++} - X_i^{--} \rangle$ or $\langle X_i^{0-} X_j^{0-} - X_i^{0+} X_j^{0+} \rangle$, which vanishes in the paramagnetic phase. In the same approximation the mixed contribution of the type (F_i^{tJ}, S_l^-) turns out to be proportional to higher-order correlation functions of the type $(X_i^{+0} X_j^{0-}, S_l^-)$ and may be neglected.

APPENDIX B: MODE-COUPPLING APPROXIMATION

Using Eq. (A1) the two-time correlation function in Eq. (14) yields 16 terms for the self-energy $\Sigma(\mathbf{q}, \omega) = \sum_{\alpha, \beta} \Sigma_{\alpha, \beta}(\mathbf{q}, \omega)$, where, e.g., $\Sigma_{JJ, JJ}(\mathbf{q}, \omega) = ((F_{\mathbf{q}}^{JJ} | (F_{\mathbf{q}}^{JJ})^+))_{\omega} / m(\mathbf{q})$. In the site representation of $\ddot{S}_{\mathbf{q}}^+$ in Eq. (14) given by Eqs. (A1)–(A7) we take into account products of three spin operators on different sites only. This is clear in the Heisenberg limit [28], where terms with coinciding sites reduce to single operators and the proper part of the correlation function in $\Sigma_{JJ, JJ}$ is considered. For finite doping, as revealed by numerical evaluations, the exclusion of terms with coinciding sites yields a better agreement with exact data than the inclusion of those terms. We calculate the two-time correlation functions in the mode-coupling approximation (see, e.g., Ref. [28]), i.e., we approximate them by a product of three single-particle two-time correlation functions as follows:

$$\begin{aligned} & \langle S_{\mathbf{k}_1}^z(t) S_{\mathbf{k}_2}^z(t) S_{\mathbf{k}_3}^-(t) S_{\mathbf{k}_1'}^z S_{\mathbf{k}_2'}^z S_{\mathbf{k}_3'}^+ \rangle \\ &= \langle S_{\mathbf{k}_1}^z(t) S_{-\mathbf{k}_1}^z \rangle \langle S_{\mathbf{k}_2}^z(t) S_{-\mathbf{k}_2}^z \rangle \langle S_{\mathbf{k}_3}^-(t) S_{-\mathbf{k}_3}^+ \rangle \\ & \times (\delta_{\mathbf{k}_1, -\mathbf{k}_1'} \delta_{\mathbf{k}_2, -\mathbf{k}_2'} + \delta_{\mathbf{k}_1, -\mathbf{k}_2'} \delta_{\mathbf{k}_2, -\mathbf{k}_1'}) \delta_{\mathbf{k}_3, -\mathbf{k}_3'}, \quad (\text{B1}) \end{aligned}$$

$$\langle X_{\mathbf{k}_1}^{0+}(t) X_{\mathbf{k}_2}^{\sigma\sigma}(t) X_{\mathbf{k}_3}^{-0}(t) X_{\mathbf{k}_1'}^{+0} X_{\mathbf{k}_2'}^{\sigma\sigma} X_{\mathbf{k}_3'}^{0-} \rangle$$

$$\begin{aligned} &= \langle X_{\mathbf{k}_1}^{0+}(t) X_{\mathbf{k}_1}^{+0} \rangle \langle X_{\mathbf{k}_2}^{\sigma\sigma}(t) X_{\mathbf{k}_2}^{\sigma\sigma} \rangle \langle X_{\mathbf{k}_3}^{-0}(t) X_{\mathbf{k}_3}^{0-} \rangle \\ & \times \delta_{\mathbf{k}_1, \mathbf{k}_1'} \delta_{\mathbf{k}_2, -\mathbf{k}_2'} \delta_{\mathbf{k}_3, \mathbf{k}_3'}. \quad (\text{B2}) \end{aligned}$$

In Ref. [25] we have shown that in the Born approximation (i.e., in the second order of the effective vertices t^2, J^2, tJ) only six contributions to the self-energy may be retained, so that

$$\begin{aligned} \Sigma(\mathbf{q}, \omega) &= \Sigma_{JJ, JJ}(\mathbf{q}, \omega) + \Sigma_{tt, tt}(\mathbf{q}, \omega) + \Sigma_{tJ, tJ}(\mathbf{q}, \omega) \\ &+ \Sigma_{Jt, Jt}(\mathbf{q}, \omega) + 2 \Sigma_{tJ, Jt}(\mathbf{q}, \omega). \quad (\text{B3}) \end{aligned}$$

The imaginary parts of the diagonal terms $\Sigma_{JJ, JJ} \equiv \Sigma_J$ and $\Sigma_{tt, tt} \equiv \Sigma_t$ are given by Eqs. (15) and (17). For one of the interference terms we obtain

$$\begin{aligned} \Sigma_{Jt, Jt}''(\mathbf{q}, \omega) &= \frac{\pi(2t)^2 (2J)^2}{m(\mathbf{q}) \omega N(\omega)} \frac{1}{N^2} \sum_{\mathbf{q}_1, \mathbf{q}_2} \Gamma_{\mathbf{q}_1 \mathbf{q}_2 \mathbf{q}_3}^2 \\ & \int_{-\infty}^{\infty} d\omega_1 d\omega_2 N(\omega_1) n(\omega_2) n(\omega - \omega_1 - \omega_2) \\ & B_{\mathbf{q}_1}(\omega_1) A_{\mathbf{q}_2}(\omega_2) A_{\mathbf{q}_3}(\omega - \omega_1 - \omega_2). \quad (\text{B4}) \end{aligned}$$

with $\Gamma_{\mathbf{q}_1 \mathbf{q}_2 \mathbf{q}_3}$ given by Eq. (16), where the contributions linear in $\gamma_{\mathbf{q}}$ reflect the exclusion of terms in \ddot{S}_i^+ with coinciding sites.

-
- [1] A.V. Chubukov, D. Pines, and J. Schmalian, in: *The Physics of Conventional and Unconventional Superconductors*, edited by K.H. Bennemann and J.B. Ketterson, (Springer Verlag, Berlin, 2004) Vol. I, p. 495. (arXiv:cond-mat/0201140).
- [2] M.A. Kastner, R.J. Birgeneau, G. Shirane, and Y. Endoh, *Rev. Mod. Phys.* **70**, 897 (1998).
- [3] P. Bourges, in: *The Gap Symmetry and Fluctuations in High Temperature Superconductors*, edited by J. Bok, G. Deutscher, D. Pavuna, and S.A. Wolf (Plenum Press, 1998), p. 349.
- [4] E. Manousakis, *Rev. Mod. Phys.* **63**, 1 (1991).
- [5] D. Manske, I. Eremin, and K.H. Bennemann, in: *The Physics of Conventional and Unconventional Superconductors*, edited by K.H. Bennemann and J.B. Ketterson (Springer-Verlag, Berlin, 2002) Vol. II, p. 731.
- [6] J. Hubbard, *Proc. R. Soc. London, Ser. A* **285**, 542 (1965).
- [7] P.W. Anderson, *Science* **235**, 1196 (1987).
- [8] Yu. A. Izyumov, *Usp. Fiz. Nauk* **167**, 465 (1997) [*Phys.-Usp.* **40**, 445 (1997)].
- [9] N.M. Plakida, *Fiz. Nizk. Temp. (Low Temp. Phys., Ukraine)* **32**, 483 (2006).
- [10] Yu. A. Izyumov and B. M. Letfulov, *J. Phys.: Condens. Matter*, **2**, 8905 (1990); Yu. A. Izyumov and J. A. Hedersen, *Int. J. Mod. Phys. B* **8**, 1877 (1994).
- [11] E. Dagotto, *Rev. Mod. Phys.* **66**, 763 (1994).
- [12] J. Jaklič and P. Prelovšek, *Advances in Physics* **49**, 1 (2000).
- [13] R. Eder, Y. Ohta, and S. Maekawa, *Phys. Rev. Lett.* **74**, 5124 (1995).
- [14] D.N. Zubarev, *Sov. Phys. Uspekhi* **3**, 320 (1960).
- [15] N.M. Plakida, *Phys. Lett. A* **43**, 481 (1973).
- [16] Yu.A. Tserkovnikov, *Theor. Math. Phys.* **49**, 993 (1981); *Theor. Math. Phys.* **52**, 712 (1982).
- [17] G. Jackeli and N. M. Plakida, *Theor. Math. Phys.* **114**, 335 (1998).
- [18] A. Sherman and M. Schreiber, *Eur. Phys. J. B* **32**, 203 (2003);
- [19] A. Sherman, *Phys. Rev. B* **70**, 184512 (2004); A. Sherman and M. Schreiber, *Fiz. Nizk. Temp. (Low Temp. Phys., Ukraine)* **32**, 499 (2006).
- [20] I. Sega, P. Prelovšek, and J. Bonča, *Phys. Rev. B* **68**, 054524, (2003).
- [21] P. Prelovšek, I. Sega, and J. Bonča, *Phys. Rev. Lett.* **92**, 027002 (2004).
- [22] A. Sherman and M. Schreiber, *Phys. Rev. B* **68**, 094519 (2003).
- [23] I. Sega and P. Prelovšek *Phys. Rev. B* **73**, 092516 (2006).
- [24] P. Prelovšek and I. Sega, *Phys. Rev. B* **74**, 214501 (2006).
- [25] A.A. Vladimirov, D. Ihle, and N. M. Plakida, *Theor. Math. Phys.* **145**, 1576 (2005).
- [26] S. Winterfeldt and D. Ihle, *Phys. Rev. B* **58**, 9402 (1998).
- [27] S. Winterfeldt and D. Ihle, *Phys. Rev. B* **56**, 5535 (1997).
- [28] S. Winterfeldt and D. Ihle, *Phys. Rev. B* **59**, 6010 (1999).
- [29] H. Shimahara and S. Takada, *J. Phys. Soc. Jpn.* **60**, 2394 (1991).
- [30] G. Jackeli and N. M. Plakida, *Phys. Rev. B* **60**, 5266

- (1999).
- [31] J. Bonča, P. Prelovšek, and I. Sega, *Europhys. Lett.* **10**, 87 (1989).
- [32] U.-J. Wiese and H.-P. Ying, *Z. Phys. B* **93**, 147 (1994).
- [33] M. Vojta and K. Becker, *Phys. Rev. B* **54**, 15483 (1996).
- [34] J. Jaklič and P. Prelovšek, *Phys. Rev. Lett.* **77**, 892 (1996).
- [35] H. Shimahara and S. Takada, *J. Phys. Soc. Jpn.* **61**, 989 (1992).
- [36] J.B. Torrance, A. Bezinge, A.I. Nazzal, T.C. Huang, S.S.P. Parkin, D.T. Keane, S.J. LaPlaca, P.M. Horn, and G.A. Held, *Phys. Rev. B* **40**, 8872 (1989).
- [37] A. Yu. Zavidonov and D. Brinkmann, *Phys. Rev. B* **58**, 12486 (1998).
- [38] S. Tyč and B. Halperin, *Phys. Rev. B* **42**, 2096 (1990).
- [39] M. Makivić and M. Jarrell, *Phys. Rev. Lett.* **68**, 1770 (1992).
- [40] D. Ihle and N. M. Plakida, *Z. Phys. B* **96**, 159 (1994).
- [41] B. Keimer, N. Belk, R.J. Birgeneau, A. Cassanho, C.Y. Chen, M. Greven, M.A. Kastner, A. Aharony, Y. Endoh, R.W. Erwin, and G. Shirane, *Phys. Rev. B* **46**, 14034 (1992).
- [42] C. Stock, W.J.L. Buyers, Z. Yamani, Z. Tun, R.J. Birgeneau, R. Liang, D. Bonn, and W.N. Hardy, *Phys. Rev. B* **77**, 104513 (2008).
- [43] K. Kakurai, S. Shamoto, T. Kiyokura, M. Sato, J.M. Tranquada, and G. Shirane, *Phys. Rev. B* **48**, 3485 (1993).
- [44] N.M. Plakida and V.S. Oudovenko, *Phys. Rev. B* **59**, 11949 (1999).
- [45] A.A. Vladimirov, D. Ihle, and N. M. Plakida, *Theor. Math. Phys.* **152**, 1331 (2007).